

Improvement in Muon Track Reconstruction with Robust Statistics

M. G. Aartsen², R. Abbasi²⁷, Y. Abdou²², M. Ackermann⁴¹, J. Adams¹⁵,
J. A. Aguilar²¹, M. Ahlers²⁷, D. Altmann⁹, J. Auffenberg²⁷, X. Bai^{31,1},
M. Baker²⁷, S. W. Barwick²³, V. Baum²⁸, R. Bay⁷, J. J. Beatty^{17,18},
S. Bechet¹², J. Becker Tjus¹⁰, K.-H. Becker⁴⁰, M. Bell³⁸,
M. L. Benabderrahmane⁴¹, S. BenZvi²⁷, J. Berdermann⁴¹, P. Berghaus⁴¹,
D. Berley¹⁶, E. Bernardini⁴¹, A. Bernhard³⁰, D. Bertrand¹², D. Z. Besson²⁵,
G. Binder^{8,7}, D. Bindig⁴⁰, M. Bissok¹, E. Blaufuss¹⁶, J. Blumenthal¹,
D. J. Boersma³⁹, S. Bohaichuk²⁰, C. Boehm³⁴, D. Bose¹³, S. Böser¹¹,
O. Botner³⁹, L. Brayeur¹³, H.-P. Bretz⁴¹, A. M. Brown¹⁵, R. Bruijn²⁴,
J. Brunner⁴¹, M. Carson²², J. Casey⁵, M. Casier¹³, D. Chirkin²⁷,
A. Christov²¹, B. Christy¹⁶, K. Clark³⁸, F. Clevermann¹⁹, S. Coenders¹,
S. Cohen²⁴, D. F. Cowen^{38,37}, A. H. Cruz Silva⁴¹, M. Danninger³⁴,
J. Daughhetee⁵, J. C. Davis¹⁷, C. De Clercq¹³, S. De Ridder²², P. Desiati²⁷,
M. de With⁹, T. DeYoung³⁸, J. C. Díaz-Vélez²⁷, M. Dunkman³⁸, R. Eagan³⁸,
B. Eberhardt²⁸, J. Eisch²⁷, R. W. Ellsworth¹⁶, S. Euler¹, P. A. Evenson³¹,
O. Fadiran²⁷, A. R. Fazely⁶, A. Fedynitch¹⁰, J. Feintzeig²⁷, T. Feusels²²,
K. Filimonov⁷, C. Finley³⁴, T. Fischer-Wasels⁴⁰, S. Flis³⁴, A. Franckowiak¹¹,
R. Franke⁴¹, K. Frantzen¹⁹, T. Fuchs¹⁹, T. K. Gaisser³¹, J. Gallagher²⁶,
L. Gerhardt^{8,7}, L. Gladstone²⁷, T. Glüsenkamp⁴¹, A. Goldschmidt⁸,
G. Golup¹³, J. A. Goodman¹⁶, D. Góra⁴¹, D. Grant²⁰, A. Groß³⁰,
M. Gurtner⁴⁰, C. Ha^{8,7}, A. Haj Ismail²², P. Hallen¹, A. Hallgren³⁹,
F. Halzen²⁷, K. Hanson¹², D. Heereman⁴², P. Heimann¹, D. Heinen¹,
K. Helbing⁴⁰, R. Hellauer¹⁶, S. Hickford¹⁵, G. C. Hill², K. D. Hoffman¹⁶,
R. Hoffmann⁴⁰, A. Homeier¹¹, K. Hoshina²⁷, W. Huelsnitz^{16,2}, P. O. Hulth³⁴,
K. Hultqvist³⁴, S. Hussain³¹, A. Ishihara¹⁴, E. Jacobi⁴¹, J. Jacobsen²⁷,
K. Jagielski¹, G. S. Japaridze⁴, K. Jero²⁷, O. Jlelati²², B. Kaminsky⁴¹,
A. Kappes⁹, T. Karg⁴¹, A. Karle²⁷, J. L. Kelley²⁷, J. Kiryluk³⁵, F. Kislak⁴¹,
J. Kläs⁴⁰, S. R. Klein^{8,7}, J.-H. Köhne¹⁹, G. Kohnen²⁹, H. Kolanoski⁹,
L. Köpke²⁸, C. Kopper²⁷, S. Kopper⁴⁰, D. J. Koskinen³⁸, M. Kowalski¹¹,
M. Krasberg²⁷, K. Krings¹, G. Kroll²⁸, J. Kunnen¹³, N. Kurahashi²⁷,
T. Kuwabara³¹, M. Labare¹³, H. Landsman²⁷, M. J. Larson³⁶,
M. Lesiak-Bzdak³⁵, M. Leuermann¹, J. Leute³⁰, J. Lünemann²⁸, J. Madsen³³,
R. Maruyama²⁷, K. Mase¹⁴, H. S. Matis⁸, F. McNally²⁷, K. Meagher¹⁶,
M. Merck²⁷, P. Mészáros^{37,38}, T. Meures¹², S. Miarecki^{8,7}, E. Middell⁴¹,

*Corresponding author. Email: wellons@icecube.wisc.edu, Phone: 304-542-4464, Address: Wisconsin Institutes for Discovery, 330 N. Orchard St., Madison, WI 53715

¹Physics Department, South Dakota School of Mines and Technology, Rapid City, SD 57701, USA

²Los Alamos National Laboratory, Los Alamos, NM 87545, USA

³also Sezione INFN, Dipartimento di Fisica, I-70126, Bari, Italy

⁴NASA Goddard Space Flight Center, Greenbelt, MD 20771, USA

37 N. Milke¹⁹, J. Miller¹³, L. Mohrmann⁴¹, T. Montaruli^{21,3}, R. Morse²⁷,
 38 R. Nahnhauser⁴¹, U. Naumann⁴⁰, H. Niederhausen³⁵, S. C. Nowicki²⁰,
 39 D. R. Nygren⁸, A. Obertacke⁴⁰, S. Odrowski³⁰, A. Olivas¹⁶, M. Olivo¹⁰,
 40 A. O’Murchadha¹², L. Paul¹, J. A. Pepper³⁶, C. Pérez de los Heros³⁹,
 41 C. Pfendner¹⁷, D. Pieloth¹⁹, N. Pirk⁴¹, J. Posselt⁴⁰, P. B. Price⁷,
 42 G. T. Przybylski⁸, L. Rädcl¹, K. Rawlins³, P. Redl¹⁶, R. Reimann¹,
 43 E. Resconi³⁰, W. Rhode¹⁹, M. Ribordy²⁴, M. Richman¹⁶, B. Riedel²⁷,
 44 J. P. Rodrigues²⁷, C. Rott¹⁷, T. Ruhe¹⁹, B. Ruzybayev³¹, D. Ryckbosch²²,
 45 S. M. Saba¹⁰, T. Salameh³⁸, H.-G. Sander²⁸, M. Santander²⁷, S. Sarkar³²,
 46 K. Schatto²⁸, M. Scheel¹, F. Scheriau¹⁹, T. Schmidt¹⁶, M. Schmitz¹⁹,
 47 S. Schoenen¹, S. Schöneberg¹⁰, L. Schönherr¹, A. Schönwald⁴¹, A. Schukraft¹,
 48 L. Schulte¹¹, O. Schulz³⁰, D. Seckel³¹, S. H. Seo³⁴, Y. Sestayo³⁰,
 49 S. Seunarine³³, C. Sheremata²⁰, M. W. E. Smith³⁸, M. Soiron¹, D. Soldin⁴⁰,
 50 G. M. Spiczak³³, C. Spiering⁴¹, M. Stamatikos^{17,4}, T. Stanev³¹, A. Stasik¹¹,
 51 T. Stezelberger⁸, R. G. Stokstad⁸, A. Stöbl⁴¹, E. A. Strahler¹³, R. Ström³⁹,
 52 G. W. Sullivan¹⁶, H. Taavola³⁹, I. Taboada⁵, A. Tamburro³¹,
 53 S. Ter-Antonyan⁶, S. Tilav³¹, P. A. Toale³⁶, S. Toscano²⁷, M. Usner¹¹,
 54 D. van der Drift^{8,7}, N. van Eijndhoven¹³, A. Van Overloop²², J. van Santen²⁷,
 55 M. Vehringer¹, M. Voge¹¹, M. Vraeghe²², C. Walck³⁴, T. Waldenmaier⁹,
 56 M. Wallraff¹, R. Wasserman³⁸, Ch. Weaver²⁷, M. Wellons^{27,*}, C. Wendt²⁷,
 57 S. Westerhoff²⁷, N. Whitehorn²⁷, K. Wiebe²⁸, C. H. Wiebusch¹,
 58 D. R. Williams³⁶, H. Wissing¹⁶, M. Wolf³⁴, T. R. Wood²⁰, K. Woschnagg⁷,
 59 C. Xu³¹, D. L. Xu³⁶, X. W. Xu⁶, J. P. Yanez⁴¹, G. Yodh²³, S. Yoshida¹⁴,
 60 P. Zarzhitsky³⁶, J. Ziemann¹⁹, S. Zierke¹, A. Zilles¹, M. Zoll³⁴, B. Recht⁴²,
 61 C. Ré⁴²

62 ¹III. Physikalisches Institut, RWTH Aachen University, D-52056 Aachen, Germany

63 ²School of Chemistry & Physics, University of Adelaide, Adelaide SA, 5005 Australia

64 ³Dept. of Physics and Astronomy, University of Alaska Anchorage, 3211 Providence Dr.,
 65 Anchorage, AK 99508, USA

66 ⁴CTSPS, Clark-Atlanta University, Atlanta, GA 30314, USA

67 ⁵School of Physics and Center for Relativistic Astrophysics, Georgia Institute of
 68 Technology, Atlanta, GA 30332, USA

69 ⁶Dept. of Physics, Southern University, Baton Rouge, LA 70813, USA

70 ⁷Dept. of Physics, University of California, Berkeley, CA 94720, USA

71 ⁸Lawrence Berkeley National Laboratory, Berkeley, CA 94720, USA

72 ⁹Institut für Physik, Humboldt-Universität zu Berlin, D-12489 Berlin, Germany

73 ¹⁰Fakultät für Physik & Astronomie, Ruhr-Universität Bochum, D-44780 Bochum,
 74 Germany

75 ¹¹Physikalisches Institut, Universität Bonn, Nussallee 12, D-53115 Bonn, Germany

76 ¹²Université Libre de Bruxelles, Science Faculty CP230, B-1050 Brussels, Belgium

77 ¹³Vrije Universiteit Brussel, Dienst ELEM, B-1050 Brussels, Belgium

78 ¹⁴Dept. of Physics, Chiba University, Chiba 263-8522, Japan

79 ¹⁵Dept. of Physics and Astronomy, University of Canterbury, Private Bag 4800,
 80 Christchurch, New Zealand

81 ¹⁶Dept. of Physics, University of Maryland, College Park, MD 20742, USA

82 ¹⁷Dept. of Physics and Center for Cosmology and Astro-Particle Physics, Ohio State
 83 University, Columbus, OH 43210, USA

84 ¹⁸Dept. of Astronomy, Ohio State University, Columbus, OH 43210, USA

85 ¹⁹Dept. of Physics, TU Dortmund University, D-44221 Dortmund, Germany

86 ²⁰Dept. of Physics, University of Alberta, Edmonton, Alberta, Canada T6G 2E1

- 87 ²¹*Département de physique nucléaire et corpusculaire, Université de Genève, CH-1211*
88 *Genève, Switzerland*
- 89 ²²*Dept. of Physics and Astronomy, University of Gent, B-9000 Gent, Belgium*
- 90 ²³*Dept. of Physics and Astronomy, University of California, Irvine, CA 92697, USA*
- 91 ²⁴*Laboratory for High Energy Physics, École Polytechnique Fédérale, CH-1015 Lausanne,*
92 *Switzerland*
- 93 ²⁵*Dept. of Physics and Astronomy, University of Kansas, Lawrence, KS 66045, USA*
- 94 ²⁶*Dept. of Astronomy, University of Wisconsin, Madison, WI 53706, USA*
- 95 ²⁷*Dept. of Physics and Wisconsin IceCube Particle Astrophysics Center, University of*
96 *Wisconsin, Madison, WI 53706, USA*
- 97 ²⁸*Institute of Physics, University of Mainz, Staudinger Weg 7, D-55099 Mainz, Germany*
- 98 ²⁹*Université de Mons, 7000 Mons, Belgium*
- 99 ³⁰*T.U. Munich, D-85748 Garching, Germany*
- 100 ³¹*Bartol Research Institute and Department of Physics and Astronomy, University of*
101 *Delaware, Newark, DE 19716, USA*
- 102 ³²*Dept. of Physics, University of Oxford, 1 Keble Road, Oxford OX1 3NP, UK*
- 103 ³³*Dept. of Physics, University of Wisconsin, River Falls, WI 54022, USA*
- 104 ³⁴*Oskar Klein Centre and Dept. of Physics, Stockholm University, SE-10691 Stockholm,*
105 *Sweden*
- 106 ³⁵*Department of Physics and Astronomy, Stony Brook University, Stony Brook, NY*
107 *11794-3800, USA*
- 108 ³⁶*Dept. of Physics and Astronomy, University of Alabama, Tuscaloosa, AL 35487, USA*
- 109 ³⁷*Dept. of Astronomy and Astrophysics, Pennsylvania State University, University Park,*
110 *PA 16802, USA*
- 111 ³⁸*Dept. of Physics, Pennsylvania State University, University Park, PA 16802, USA*
- 112 ³⁹*Dept. of Physics and Astronomy, Uppsala University, Box 516, S-75120 Uppsala, Sweden*
- 113 ⁴⁰*Dept. of Physics, University of Wuppertal, D-42119 Wuppertal, Germany*
- 114 ⁴¹*DESY, D-15735 Zeuthen, Germany*
- 115 ⁴²*Dept. of Computer Sciences, University of Wisconsin, Madison, WI 53706, USA*

116 **Abstract**

117 The IceCube detector is a high-energy neutrino telescope located at the geo-
118 graphic South Pole. Neutrinos cannot be directly observed and must be inferred
119 from their interactions with other particles. These interactions sometimes gener-
120 ate a muon, which in turn emits observable light. At the energies the IceCube
121 detector is sensitive to, the neutrino and generated muon have almost parallel
122 tracks, so the neutrino track can be extrapolated from a reconstruction of the
123 muon track. However, reconstructing the muon track from the observed light is
124 challenging due to noise, light scattering in the ice medium, and the possibility
125 of simultaneously having multiple muons inside the detector.

126 This manuscript describes our work on two problems: (1) the *track recon-*
127 *struction* problem, in which, given a set of observations, our goal is to recover
128 the track of a muon, and (2) the *coincident event* problem, which is to deter-
129 mine how many muons are active in the detector during a time window. Rather
130 than solving these problems by developing more complex physical models, our
131 approach is to augment the detector's current models with simple filters and
132 robust statistical techniques. Using the metric of median angular resolution,
133 a standard metric for track reconstruction, our solution improves the accuracy

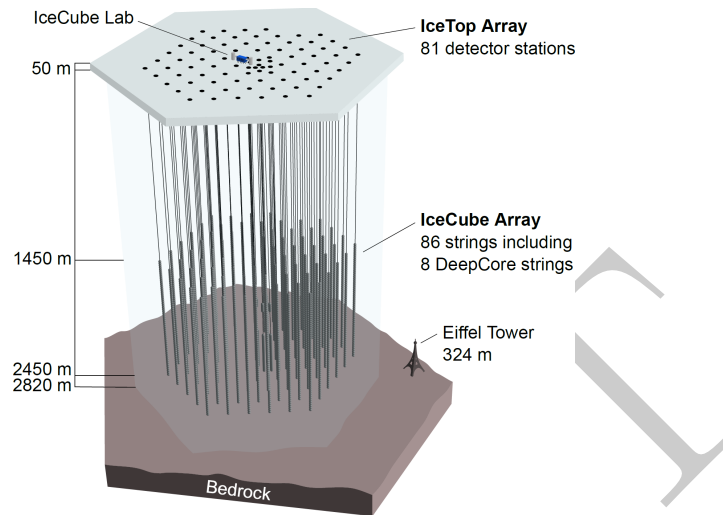


Figure 1: The IceCube neutrino detector in the Antarctic ice. A picture of the Eiffel Tower is shown for scale.

134 in the reconstruction direction by 13%. Our solution for the coincident-event
 135 problem accurately determines the number of muons 98% of the time, which is
 136 an improvement of 86% over the software previously used in IceCube.

137 *Keywords:* IceCube, Track reconstruction, Neutrino telescope, Neutrino
 138 astrophysics, Robust Statistics

139 **1. Introduction**

140 The IceCube neutrino detector searches for neutrinos that are generated by
 141 the universe’s most violent astrophysical events: exploding stars, gamma ray
 142 bursts, and cataclysmic phenomena involving black holes and neutron stars [1].
 143 The detector, roughly a cubic kilometer in size, is located near the geographic
 144 South Pole and is buried to a depth of about 2.5 km in the Antarctic ice [2].
 145 The detector is illustrated in Figure 1 and a more complete description is given
 146 in Section 2.

147 When a neutrino enters the telescope, it sometimes interacts with the ice and
 148 generates a muon. The neutrino track can be extrapolated from a reconstruction
 149 of the muon track. Muons are also be generated by cosmic rays, and separation
 150 of the cosmic ray muons and neutrino muons is a necessary step for neutrino
 151 analysis. This separation is challenging, as the number of observed cosmic
 152 ray muons exceeds the number of observed neutrino muons by five orders of
 153 magnitude [3].

154 The primary mechanism for separating the cosmic ray muons from the neu-
155 trino muons is reconstructing the muon track, and determining if the muon was
156 traveling downwards into the Earth or upwards out of the Earth. Since neu-
157 trinos can penetrate the Earth but cosmic ray muons cannot, it follows that a
158 muon traveling out of the Earth must have been caused by a neutrino. Thus,
159 by selecting only the muons that are reconstructed as up-going, the cosmic ray
160 muons can, in principle, be removed from the data. Since the neutrino muon
161 are dominated by cosmic ray muons, high accuracy reconstructions are critical
162 for preventing erroneously reconstructed cosmic ray muons from dominating the
163 neutrino analysis.

164 We examine two problems that arise in the IceCube detector’s separation of
165 cosmic rays muons from neutrino muons:

- 166 1. *Reconstruction*, in which the track of a muon is reconstructed from the
167 observed light at different positions and times in the detector.
- 168 2. *Coincident Event Detection*, in which we detect the number of muons
169 inside the detector, and assign observed photons to a muon.

170 The IceCube Collaboration has spent considerable effort on both of these
171 problems over the last decade, as they are a critical step for data analysis.
172 They have developed sophisticated domain models that take into account the
173 interaction of near- and far-field effects of light, and have undertaken complex
174 mapping efforts to understand the effects of photon propagation in the ice [3,
175 4]. Our solutions do not further refine the detailed modeling of these physical
176 effects, but instead augment the models with off-the-shelf statistical techniques
177 combined with some simple data filtering to remove outliers.

178 *Related Work.* Track reconstruction and coincident event detection challenges
179 are ubiquitous in particle physics [5–7], both in particle accelerators and cosmic
180 particle detectors. While the work described in this manuscript builds on the
181 previous technique developed for the IceCube detector [3], our techniques are
182 general purpose, and potentially have applications in detectors beyond IceCube.

183 *Outline.* We begin by describing the necessary background on the IceCube de-
184 tector in Section 2. In Section 3, we describe the reconstruction pipeline in-
185 cluding the prior IceCube software, then we discuss our work and its results.
186 Section 4 describes our work on coincident event detection, and follows a parallel
187 structure to Section 3. We describe how in this application, a simple heuristic
188 approach is an improvement over the prior software. We close with a conclusion
189 in Section 5.

190 2. Background

191 The IceCube detector is composed of 5160 optical detectors, each composed
192 of a photomultiplier tube (PMT) and onboard digitizer[8]. The PMTs are spread
193 over 86 vertical strings arranged in a hexagonal shape, with a total instrumented

194 volume of approximately a cubic kilometer. The PMTs on a given string are sep-
195 arated vertically by 17 m, and the string-to-string separation is roughly 125 m.

196 As the muon travels through the detector, it radiates light [9], which is ob-
197 served by the PMTs and broken down into discrete *hits* [10]. A collection of
198 hits is called an *event*, and if the number of hits in an event is sufficiently large,
199 the muon track reconstruction algorithm is triggered.

200 The track reconstruction algorithms used in the detector have several chal-
201 lenges which must be overcome. The underlying mechanics are stochastic and
202 incompletely modeled, the data is noisy and contains outliers, and the compu-
203 tational abilities of the detector are limited.

204 *Modeling Difficulties.* The underlying physics of the system are nontrivial to
205 model. The muon's light is scattered by the dust and air crystals in the ice
206 medium. This scattering is both complex and stochastic, and the scattering
207 properties of the ice vary with depth [11].

208 *Noise.* An unescapable challenge is the noise inherent in the data. The PMTs
209 are so sensitive to light that they can record hits even in the absence of nearby
210 muons. These hits can arise from photons generated either by radioactive decay
211 inside the PMT [12] of the ice.

212 *Computational Constraints.* The reconstruction algorithms are also limited in
213 complexity by the computing resources available at the South Pole. The track
214 reconstruction algorithm has to process about 3000 muons per second, so algo-
215 rithms with excessive computational demands are discouraged.

216 3. Reconstruction Problem

217 By augmenting the reconstruction algorithm with some simple filters and
218 classical data analysis techniques, we show significant improvement in the re-
219 construction algorithm's accuracy.

220 3.1. Prior IceCube Software

221 The muon track reconstruction process (outlined in Figure 2) starts when the
222 number of detected hits exceeds a preset threshold and initiates data collection.
223 After the initial data is collected, it then passes through a series of simple filters
224 to remove obvious outliers, described more in [13].

225 This is followed by a simple reconstruction algorithm *linefit*, which simply
226 finds the track that minimizes the sum of the squares of the distances between
227 the track and the hits. More formally, assume there are N hits, and denote
228 the position and time of the i th hit as \vec{x}_i and t_i respectively. Let the recon-
229 structed muon track have a velocity of \vec{v} , and let the reconstructed track pass
230 through point \vec{x}_0 at time t_0 . Then linefit reconstruction solves the *least-squares*
231 optimization problem

$$\min_{t_0, \vec{x}_0, \vec{v}} \sum_{i=1}^N \rho_i(t_0, \vec{x}_0, \vec{v})^2, \quad (1)$$

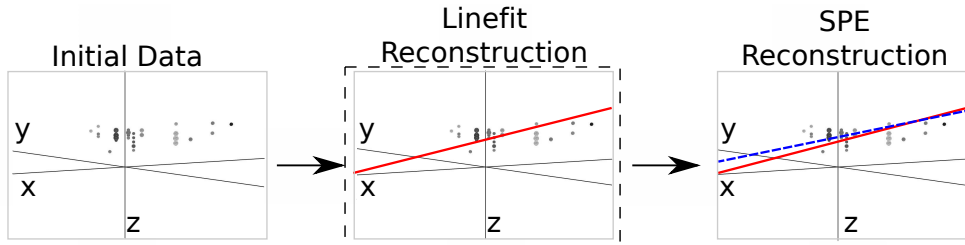


Figure 2: The reconstruction pipeline used to process data in the IceCube detector. After initial data is collected, it is then processed by some simple noise filters, which remove clear outliers. This cleaned data is processed by a simple reconstruction algorithm (solid line), which is used as the seed for the more sophisticated reconstruction algorithm (dashed line). The sophisticated reconstruction is then evaluated as a potential neutrino. Our work in the reconstruction problem makes changes to the simple reconstruction step (indicated by the dashed box).

232 where

$$\rho_i(t_0, \vec{x}_0, \vec{v}) = \|\vec{v}(t_i - t_0) + \vec{x}_0 - \vec{x}_i\|_2. \quad (2)$$

233 The linefit reconstruction is primarily used to generate an initial track or *seed*
 234 for a more sophisticated reconstruction.

235 The reconstruction algorithm for the sophisticated reconstruction is *Single-*
 236 *Photo-Electron-Fit (SPE)* [3]. SPE uses the least-squares reconstruction, the
 237 event data, and a parameterized probability distribution function of scattering
 238 in ice [3] to reconstruct the muon track.

239 3.2. Algorithm Improvement

240 SPE is dependent on the seed. Given a seed that is inaccurate by greater
 241 than or equal to 6° , SPE typically cannot recover, and produces a reconstruction
 242 with the same level of inaccuracy as the seed track. In addition, the likelihood
 243 space for SPE can contain multiple local maxima, so improving the accuracy of
 244 a seed already near the true solution still improves the accuracy of SPE. Thus,
 245 we focused our work on improving the quality of the seed.

246 As indicated in Equation 1, a least-squares fit models the muon as a single
 247 point moving in a straight line, and hits are penalized quadratically in their
 248 distance from this line. Thus there is an implicit assumption in this model,
 249 which is that all the hits will be near the muon. There are several pitfalls in
 250 this assumption:

- 251 1. It ignores the scattering effects of the ice medium. Some of the photons can
 252 scatter for over a microsecond, which means that when they are recorded
 253 by a PMT, the muon will be over 300 m away.
- 254 2. While the noise reduction steps remove most of the outlier noise, the noise
 255 hits that survive can be far from the muon. Since these outliers are given
 256 quadratic weight, they exert a huge influence over the model.

257 The first pitfall is a case of the model being incomplete and not modeling
 258 the data, and the second amounts to the model not being robust to noise. Our
 259 solution was twofold: improve the model and increase the noise robustness by
 260 replacing least squares with robust statistical techniques.

261 3.2.1. Improving the Model

262 The least-squares model does not model the scattering, and thus hits gener-
 263 ated by photons that scattered for a significant length of time are not useful
 264 predictors of the muon’s position. We found that a simple filter could identify
 265 these scattered hits, and generate an accuracy improvement of almost a factor
 266 of two by removing them from the dataset.

267 More formally, for each hit h_i , the algorithm looks at all neighboring hits
 268 within a neighborhood of r , and if there exists a neighboring hit h_j with a time
 269 stamp that is t earlier than h_i , then h_i is considered a scattered hit, and is not
 270 used in the simple reconstruction algorithm. Optimal values of r and t were
 271 found to be 156 m and 778 ns by tuning them on simulated muon data.

272 3.2.2. Adding Robustness to Noise

273 As described in equation 1, the least squares model gives outliers quadratic
 274 weight, whereas we would prefer that outliers had zero weight. There are robust
 275 models in classical statistics designed to marginalize outliers. We experimented
 276 replacing the least-squares model with a Huber fit [14], which improved the
 277 reconstruction accuracy.

278 More formally, we replace Equation 1 with the optimization problem

$$\min_{t_0, \vec{x}_0, \vec{v}} \sum_{i=1}^N \phi(\rho_i(t_0, \vec{x}_0, \vec{v})), \quad (3)$$

279 where the Huber penalty function $\phi(\rho)$ is defined as

$$\phi(\rho) \equiv \begin{cases} \rho^2 & \text{if } \rho < \mu \\ \mu(2\rho - \mu) & \text{if } \rho \geq \mu \end{cases} . \quad (4)$$

280 Here, $\rho_i(t_0, \vec{x}, \vec{v})$ is defined in Equation 2 and μ is a constant calibrated to the
 281 data (on simulated muon events, the optimal value of μ is 153 m).

282 The Huber penalty function has two regimes. In the near-hit regime ($\rho < \mu$)
 283 hits are assumed to be strongly correlated with the muon’s track, and the Huber
 284 penalty function behaves like least squares, giving these hits quadratic weight.
 285 In the far-hit regime ($\rho \geq \mu$), hits are given linear weights as they are more
 286 likely to be noise.

287 In addition to its attractive robustness properties, the Huber fit’s weight
 288 assignment also has the added benefit that it inherently labels points as outliers
 289 (those with $\rho \geq \mu$). Thus, once the Huber fit is computed, we can go one step
 290 farther and simply remove the labeled outliers from the dataset. A better fit is
 291 then obtained by computing the least-squares fit on the data with the outliers
 292 removed. The entire algorithm has a mean runtime that is approximately six
 293 times slower than Linefit’s mean runtime.

Table 1: Median angular resolution (degrees) for reconstruction improvements. The first line is the accuracy of the prior least-squares model, and the subsequent lines are the accuracy measurements from cumulatively adding improvements into the simple reconstruction algorithm.

Algorithm	θ_{med}
Linefit Reconstruction (Least-Squares)	9.917
With Addition of Logical Filter	5.205
With Addition of Huber Regression	4.672
With Addition of Outlier Removal	4.211

294 3.3. Results

295 Our goal is to improve the accuracy of the reconstruction in order to better
 296 separate neutrinos from cosmic rays. Thus we present three measurements: (1)
 297 the accuracy change between linefit and the new algorithm, (2) the accuracy
 298 change when SPE is seeded with the new algorithm instead of linefit, and (3)
 299 the improvement in separation between neutrinos and cosmic rays.

300 To measure the improvement generated by our changes, we use the metric of
 301 *median angular resolution* θ_{med} , which is a standard metric used in the collab-
 302 oration. The angular resolution of a reconstruction is the arc-distance between
 303 the reconstruction and the true track. Our dataset is drawn from simulated
 304 neutrino data designed to be similar to that observed by the detector.

305 We can improve the median angular resolution of the simple reconstruction
 306 by 57.6%, as shown in Table 1. Seeding SPE with the improved simple recon-
 307 struction generates an improvement in the angular resolution of 12.9%. These
 308 improvements in the reconstruction algorithm result in 10% fewer atmospheric
 309 muons erroneously reconstructed as up-going, and 1% more muons correctly
 310 reconstructed as up-going.

311 4. Coincident Event Problem

312 In our second experiment, we look at the problem of determining when more
 313 than one muon has entered the detector. In the most common case, a single
 314 muon will pass through the detector and generate an event before exiting. These
 315 events are processed by the pipeline described in Figure 2. However, for roughly
 316 9% of the events collected by the data collection algorithm, more than one muon
 317 will be passing through the detector simultaneously, an occurrence known as a
 318 *coincident event*.

319 One of the primary sources of background noise in the scientific analyses
 320 of the IceCube Collaboration is coincident background muons that have been
 321 erroneously reconstructed as neutrinos. To see why this occurs, consider the
 322 coincident event shown in Figure 3. There are two clear groups of hits; how-
 323 ever, the reconstruction algorithm treats them as a single group, resulting in a
 324 erroneous reconstruction. In the ideal case, the reconstruction algorithm would
 325 identify coincident events and split them, as in Figure 4.

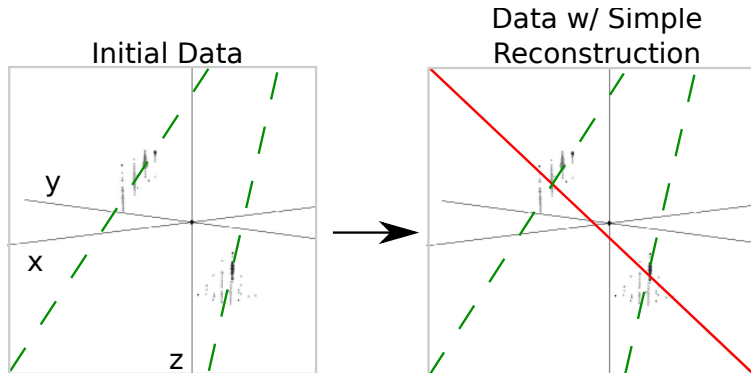


Figure 3: In this example, an event that is clearly composed of two muons (actual tracks shown as dashed lines) is treated as a single muon, and thus the reconstruction (solid line) is inaccurate.

326 The challenge in this example is determining the number of muons in an
 327 event. In our results, we find that a simple spatial clustering algorithm can
 328 solve this classification problem with less than 2% error.

329 4.1. Prior IceCube Software

330 Coincident events have been a concern in the IceCube analysis [15] for years,
 331 and some software has been developed to handle coincident events. As a baseline
 332 of comparison, we use the *TTrigger* software, which is described in [16].

333 4.2. Algorithm Improvement

334 Our solution to this problem is a proximal clustering algorithm. The intu-
 335 ition in proximal clustering is that points local in space and time are probably
 336 from the same muon. The proximal clustering algorithm iterates through each
 337 pair of hits (i, j) and builds an adjacency matrix \mathbf{A} as

$$\mathbf{A}_{ij} = \begin{cases} 1 & \text{if } \|\Delta x^2 + \Delta y^2 + \Delta z^2 + (c\Delta t)^2\|_2 \leq \alpha, \\ 0 & \text{otherwise} \end{cases} \quad (5)$$

338 where $\Delta x, \Delta y, \Delta z$ and Δt are the space and time differences between the pair
 339 of hits, and α is tuned to the data (in this application, the optimal value of
 340 α is 450 m). The clustering can be recovered by extracting the connected
 341 components of the graph defined by \mathbf{A} . A connected component of a graph is a
 342 subgraph such that there exist a path between any two vertices of this subgraph.

343 4.2.1. Improving the Model

344 When implemented naively, proximal clustering succeeded for the majority
 345 of the events, but failed if there was a gap in the muon track, which can occur
 346 when the muon travels through dusty ice. If there is a significantly large gap,
 347 the algorithm erroneously separates the hits into two clusters.

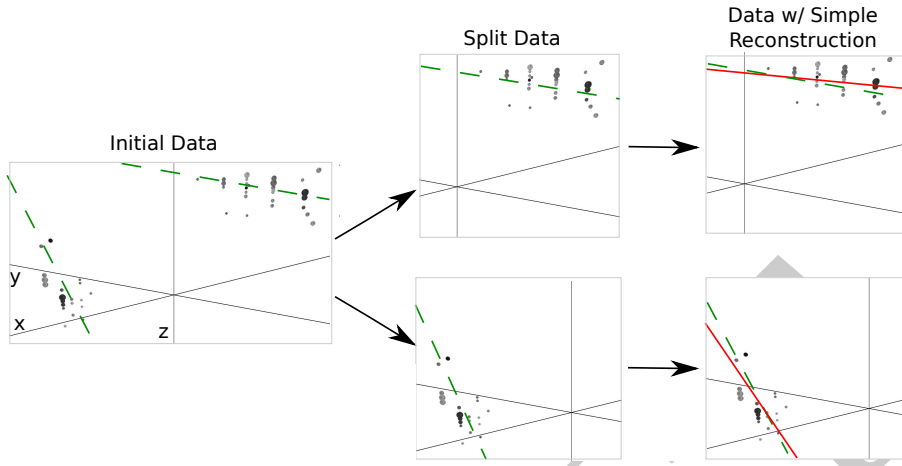


Figure 4: Ideally, the detector would split coincident events before computing the reconstruction. Splitting the event results in more accurate reconstructions (reconstructions shown as solid lines, true muon tracks shown as dashed lines). Note the difference in the reconstructions compared with Figure 3.

348 To get around this, an additional heuristic is added, *track connecting*. After
 349 the data segmentation is finished, track connecting determines if separate
 350 clusters should be combined. It computes the mean position and time of each
 351 cluster, and connects a hypothetical muon track T between each pair of sub-
 352 spaces.

353 It checks if the speed s of the hypothetical track is within 25% of the speed
 354 of light c , and it checks that the mean distance between hits and T in both
 355 clusters is less than 60 m. If T passes both checks, the clusters are combined.

356 4.2.2. Adding Robustness to Noise

357 Proximal clustering is susceptible to noise. Noise hits close to two disjoint
 358 tracks will be considered adjacent to both tracks, and thus can connect the two
 359 tracks in the adjacency matrix.

360 One heuristic that worked well at mitigating this problem was to not use
 361 all the hits in building the adjacency matrix. During data collection, some hits
 362 are flagged as having a *local coincidence condition*, which indicates that both
 363 they and a neighboring PMT reported a hit. These hits have a high probability
 364 of not being noise hits, and thus exclusively using them to build the adjacency
 365 matrix mitigates the problem of erroneously connecting two tracks.

366 After the proximal clustering algorithm has extracted the tracks from the
 367 adjacency matrix, the hits not used in the construction of the adjacency matrix
 368 are simply assigned to the closest reconstructed track.

369 4.3. Results

370 There were two competing goals for coincident event detection algorithms:
 371 the algorithm should be conservative enough that events containing single tracks

Table 2: Error Rates for Classification Algorithms

Algorithm	$E_{\text{Single}} \%$	$E_{\text{Multiple}} \%$	$E_{\text{tot}} \%$
Trivial	0.0	100.0	8.3
TTrigger	11.5	31.8	13.2
Proximal clustering	0.2	18.9	1.8

372 are not erroneously split, and aggressive enough that a useful fraction of coin-
373 cident events are split correctly. Erroneously discarding events containing neu-
374 trinos is worse than erroneously allowing additional noise into the data pool,
375 as noise can be eliminated by future filtering of the data pool. Our algorithm
376 is tuned to keep almost all of the single events correctly unsplit, while still
377 correctly splitting 80% of the coincident events.

378 4.3.1. Measurements

379 We modified the reconstruction pipeline shown in Figure 2, in between the
380 noise cleaning and the simple reconstruction, by adding a step for coincident
381 event detection, as shown in Figure 4. This step takes cleaned data and attempts
382 to classify the event as a single-track or multiple-track event.

383 We ran each algorithm on two datasets of simulated data. One dataset
384 comprised single-muon events, and the other dataset comprised multiple-muon
385 events. In each dataset, we measured the classification error E , which is the
386 fraction of events that were misclassified. To get a global measurement, we
387 compute the *total error* E_{tot} , defined as

$$E_{\text{tot}} = w_{\text{Single}} E_{\text{Single}} + w_{\text{Multiple}} E_{\text{Multiple}}. \quad (6)$$

388 For computing E_{tot} , we use $w_{\text{Single}} = 0.917$ and $w_{\text{Multiple}} = 0.083$, which is
389 the frequency in which single-muon and multiple-muon events appear in data
390 simulating the distribution of events that trigger the reconstruction algorithm.

391 We present our results for the coincident event problem by measuring how
392 well each algorithm performs at determining the number of subspaces in an
393 event.

394 There are two natural comparisons for our work: the prior software TTrigger,
395 as well as the trivial algorithm, which always classifies each event as a single-
396 track event. Clearly, the latter will always get the single-track events correct,
397 and always get the multiple-track events wrong. We provide a comparison of
398 these techniques in Table 2. As shown, our software classifies the number of
399 muons in the detector 86% better than TTrigger.

400 5. Conclusions

401 The challenges in the IceCube detector are complex. Despite this complexity,
402 we found that we can achieve significant improvement via classical data analysis
403 algorithms and simple models.

404 We looked at the problem of general reconstruction improvement, and found
405 that by applying a simple filter to the data and adding some robustness to the
406 fitting algorithm, we got superior reconstructions in the noisy environments of
407 the IceCube data. Our reconstruction software runs on-site, and is included in
408 all IceCube analysis.

409 We also looked at the problem of determining the number of muons in the
410 detector. We found that proximal clustering, the simplest algorithm that we
411 tried, was as good as or better than all other tested algorithms. Our proximal
412 clustering algorithm was an 86% improvement over the current software.

413 References

- 414 [1] IceCube Collaboration, IceCube webpage, <http://icecube.wisc.edu/>.
- 415 [2] IceCube Collaboration, First year performance of the IceCube neutrino
416 telescope, *Astroparticle Physics* 26 (3) (2006) 155–173.
- 417 [3] IceCube Collaboration, Muon track reconstruction and data selection tech-
418 niques in AMANDA, *Nuclear Instruments and Methods in Physics Re-*
419 *search Section A* 524 (2004) 169–194.
- 420 [4] IceCube Collaboration, Measurement of South Pole ice transparency with
421 the IceCube LED calibration system IceCube Collaboration, *Nuclear In-*
422 *struments and Methods in Physics Research Section A*.
- 423 [5] ATLAS Collaboration, Tracking and vertexing with the ATLAS detector at
424 the LHC, *Nuclear Instruments and Methods in Physics Research Section A:*
425 *Accelerators, Spectrometers, Detectors and Associated Equipment* 650 (1)
426 (2011) 218–223.
- 427 [6] R. S. Chivukulaa, M. Goldena, E. H. Simmons, Multi-jet physics at hadron
428 colliders, *Nuclear Physics B* 363 (1) (1991) 83–96.
- 429 [7] S. Ellis, J. Huston, K. Hatakeyama, P. Loch, M. Tönnesmann, Jets in
430 hadron–hadron collisions, *Progress in Particle and Nuclear Physics* (60)
431 (2008) 484–551.
- 432 [8] IceCube Collaboration, Calibration and characterization of the IceCube
433 photomultiplier tube, *Nuclear Instruments and Methods in Physics Re-*
434 *search Section A* 618 (2010) 139–152.
- 435 [9] IceCube Collaboration, An improved method for measuring muon energy
436 using the truncated mean of dE/dx , *Nuclear Instruments and Methods in*
437 *Physics Research Section A*.
- 438 [10] IceCube Collaboration, The icecube data acquisition system: Signal cap-
439 ture, digitization, and timestamping, *Nuclear Instruments and Methods in*
440 *Physics Research Section A* 601 (3) (2009) 294–316.

- 441 [11] M. Wolf, E. Resconi, Verification of South Pole glacial ice simulations in Ice-
442 Cube and its relation to conventional and new, accelerated photon tracking
443 techniques, Master's thesis, Max-Planck-Institut für Kernphysik Heidelberg
444 (September 2010).
- 445 [12] IceCube Collaboration, IceCube sensitivity for low-energy neutrinos from
446 nearby supernovae, *Astronomy & Astrophysics* 535 (A109) (2011) 18.
- 447 [13] M. Ackermann, Searches for signals from cosmic point-like sources of high
448 energy neutrinos in 5 years of AMANDA-II data, Ph.D. thesis, Humboldt-
449 Universität zu Berlin (2006).
- 450 [14] S. Boyd, L. Vandenberghe, *Convex Optimization*, Cambridge University
451 Press, 2009.
- 452 [15] IceCube Collaboration, Measurement of the atmospheric neutrino energy
453 spectrum from 100 GeV to 400 TeV with IceCube, *Physical Review D*
454 83 (1).
- 455 [16] D. Chirkin, Measurement of the atmospheric neutrino energy spectrum
456 with IceCube, Proceedings of the 31st ICRC.